Geomechanics and Engineering, *Vol. 29, No. 5 (2022) 509-522*
https://doi.org/10.12989/gae.2022.29.5.509

Field test and numerical study of the effect of shield tail-grouting parameters on surface settlement

Xiaokang Shao[a], Zhiyong Yang*, Yusheng Jiang[b], Xing Yang[c] and Weiqiang Qi[d]

School of Mechanics and Civil Engineering, China University of Mining and Technology-Beijing, Ding, No. 11 Xueyuan Road, Haidian District, Beijing 100083, P.R. China

(Received January 31, 2022, Revised April 14, 2022, Accepted April 26, 2022)

Abstract. Tail-grouting is an effective measure in shield engineering for filling the gap at the shield tail to reduce ground deformation. However, the gap-filling ratio affects the value of the gap parameters, leading to different surface settlements. It is impossible to adjust the fill ratio indiscriminately to study its effect, because the allowable adjustment range of the grouting quantity is limited to ensure construction site safety. In this study, taking the shield tunnel section between Chaoyanggang Station and Shilihe Station of Beijing Metro Line 17 as an example, the correlation between the tail-grouting parameter and the surface settlement is investigated and the optimal grouting quantity is evaluated. This site is suitable for conducting field tests to reduce the tail-grouting quantity of shield tunneling over a large range. In addition, the shield tunneling under different grouting parameters was simulated. Furthermore, we analyzed the evolution law of the surface settlement under different grouting parameters and obtained the difference in the settlement parameters for each construction stage. The results obtained indicate that the characteristics of the grout affect the development of the surface settlement. Therefore, reducing the setting time or increasing the initial strength of the grout could effectively suppress the development of surface subsidence. As the fill ratio decreases, the loose zone of the soil above the tunnel expands, and the soil deformation is easily transmitted to the surface. Meanwhile, owing to insufficient grout support, the lateral pressure on the tunnel segments is significantly reduced, and the segment moves considerably after being removed from the shield tail.

Keywords: grout hardening properties; grouting quantity; shield tunnel; surface settlement; tail-grouting

1. Introduction

Avoiding surface deformation during shield tunnel construction is challenging. It has been found that the deformation caused by tunnel excavation predominantly depends on the following factors: (1) stratum type and groundwater, (2) buried depth and diameter of the tunnel, and (3) details of the construction (Peck 1969). Tail-grouting is a vital construction measure used to control stratum deformation in shield engineering, and it has a significant impact on construction quality. The grout is used to fill the construction gap at the tail of the shield during tunneling. Lo and Rowe (1982) and Rowe and Kack (1983) introduced gap parameters to evaluate surface settlement, by considering factors such as the soil volume loss, physical gap of the tunnel excavation, and construction quality. As shown in Fig. 1, the gap between the outer surface of the segment and the soil around the tunnel consists of the following parts: (1) gap between the excavation boundary and the shield shell, (2) thickness of the shell itself, and (3) gap between the inner surface of the shell and the outer surface of the segment.

In shield tunneling, the grout is used to fill the construction gap. However, the gap-filling ratio affects the value of the gap parameters, leading to different surface settlements. Owing to the unevenness of the stratum (cracks and pores in the soil), grouting pressure fluctuations, loss of slurry in the pipeline, and volume change during the grout-hardening process, it is only theoretically possible to fill the construction gap (Li *et al.* 2017, Xu *et al.* 2020). Moreover, the filling is often non-uniform.

In recent years, researchers have been focusing on the filling ratio of the shield tunnel synchronous grouting. Zhang *et al*. (2010), Yu *et al*. (2016), and Wang *et al*. (2020) used radar radiofrequency and acoustic emission technology to scan the filling thickness of the grout behind the segment. This technology can evaluate the quality of the tail-grouting and segment. Extensive research revealed that the tail-grouting behavior of the shield construction has three parameters that need to be considered: grouting pressure, grouting quantity, and hardening time. Lavasan *et al*. (2018) and Do *et al*. (2014) used numerical simulation methods to study the influence of grouting pressure on the ground displacement, pore pressure, and lining internal forces. Kavvadas *et al*. (2017) established a three-dimensional finite element model of the shield excavation to study surface settlements under different grouting pressures. Liu *et al*. (2020) and Ding *et al*. (2019) carried out a model test

*Corresponding author, Assistant Professor
E-mail: yangzy1010@126.com
[a]Ph.D. Student
[b]Ph.D.
[c]Ph.D. Student
[d]Ph.D. Student

ISSN: 2005-307X (Print), 2092-6219 (Online)

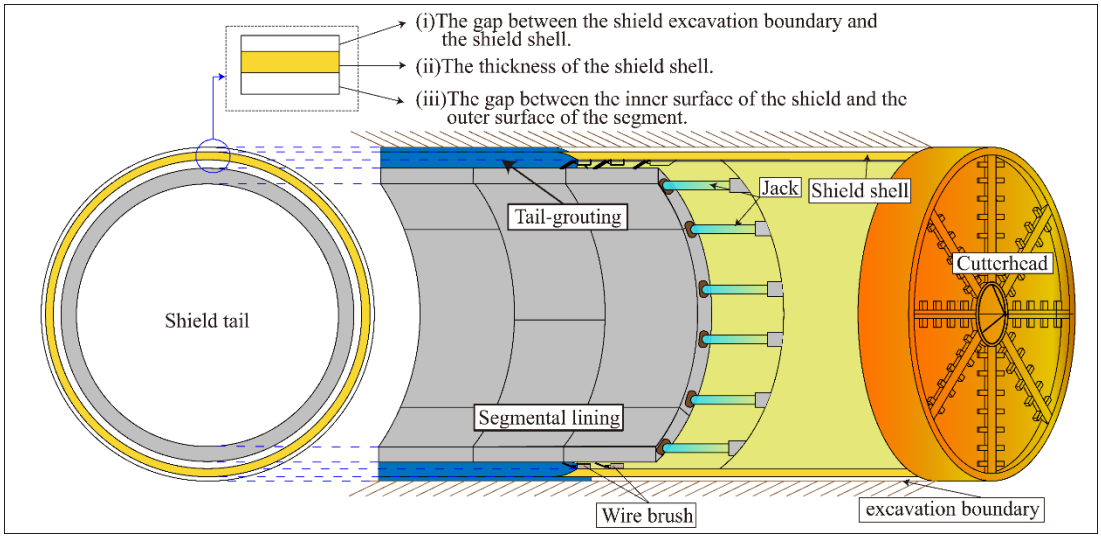

Fig. 1 Schematic illustration of construction gap in shield tunneling

Table 1 Soil parameters

Layer name	h	γ_{sat}	c	φ	E	ν	K_0
	m	kN/m^3	kPa	°	MPa	-	-
Fill	2	19	8	0	4.2	0.35	0.42
③$_1$Silty clay	3	18.8	41	7	8	0.35	0.34
③Clayey silt	7	19.4	11	12	18.9	0.3	0.40
④$_3$Silty sand	5	20	0	15	20	0.3	0.36
⑥Silty clay	10	18.9	59	10	10	0.3	0.38
⑦$_1$Coarse sand	5	21	0	30	60	0.3	0.32
⑧$_1$Clay	10	18.2	50	15	12	0.3	0.38
⑨$_1$Fine sand	8	19.6	0	35	50	0.35	0.34

of shield tunneling and obtained the influence law of the tail-grouting on the ground surface settlement. Zhao *et al*. (2019) conducted a large-scale model test and numerical simulations to analyze the difference in the surface settlements induced by different hardening time of the grout. Li (2020) adjusted the grouting volume and pressure within the allowable construction range, studied the relationship between the two parameters and the surface deformation, and obtained the best grouting pressure and volume when the surface did not settle or uplift.

Compared with the change in the grouting pressure, the fill ratio of grouting has a more direct effect on the surface settlement. However, substantially reducing the tail-grouting quantity generally cause an increase in stratum deformation and even surface collapse. Therefore, field tests are rarely conducted. In this regard, we selected the shield tunnel section between Chaoyanggang Station and Shilihe Station on Beijing Metro Line 17 as an example.

For this project, the soil was excavated after the tunnel segment was assembled and the tunnel was expanded into a station. Therefore, the soil failure caused by insufficient grouting was allowed in this project. Based on the field test of the tail-grouting, this study also obtained more correlations between the tail-grouting parameters and the surface settlements using numerical simulation. In this study, a method to evaluate the optimal grouting quantity as well as the influence of the characteristics of the grout on the development of the surface settlement was developed. It can provide a reference for the selection of tail-grouting parameters in shield engineering.

2. Tail-grouting field test

2.1 Review of the test tunnel

The tunnel section between Chaoyanggang Station and Shilihe Station on Beijing Metro Line 17 is approximately 3.7 km. The earth pressure balance shield (EPBS) in this project was manufactured by the China Railway

Construction Heavy Industry Group. The excavation diameter is 6640 mm. The tunnel uses a concrete segment with an outer diameter of 6400 mm, an inner diameter of 5600 mm, and a width of 1200 mm as the lining structure. As shown in Fig. 2, at the request of the surrounding residents, a new metro station (Shibalidian Station) needed to be added in the middle of the tunnel section (located at the 1562nd–1822nd ring of the left line). To shorten the construction period, the underground diaphragm wall of the Shibalidian Station was built before the shield arrived. The two underground walls use glass fiber reinforcement instead of steel bars at the positions where the tunnel passes, which

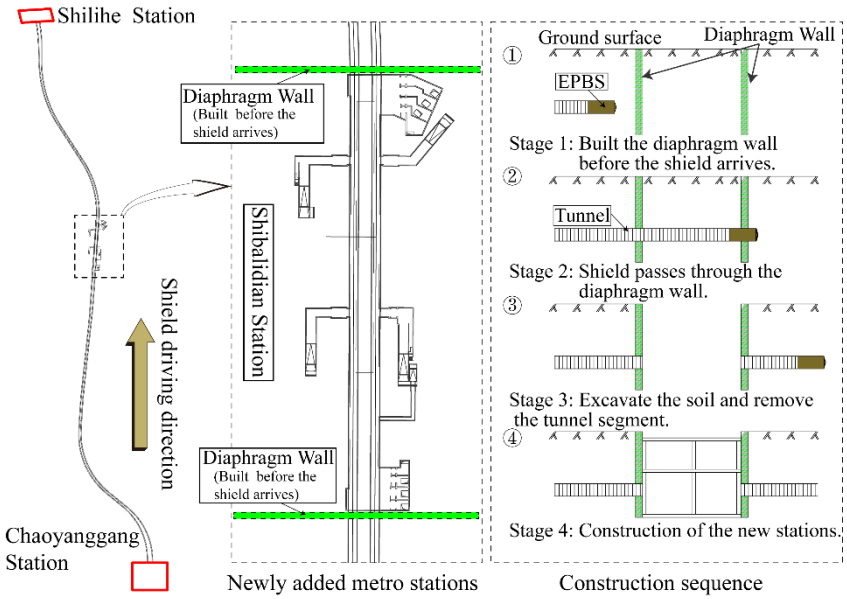

Fig. 2 Plan of the tunnel section and construction steps of newly added stations

can ease the passage of the shield through the walls of the station. After the shield was driven out of the newly added station, the soil covering the tunnel and the tunnel segments was removed to realize the construction of the new station and the tunnel section simultaneously without any mutual interference. The geological conditions of the newly-added station are shown in Fig. 3. The buried depth of the tunnel is 11 m, and the crossing strata are clayey silt, silty sand, and silty clay. The buried depth of the groundwater level is within 22–27 m. The parameters of the soil layer obtained via on-site tests and conventional laboratory tests are listed in Table 1.

2.2 Parameters of tail gap grouting

2.2.1 Calculation of reasonable grouting pressure

As the shield advances, grout is injected into the gap between the shield tail and the surrounding soil through the synchronous grouting hole; the sprayed grout pressure induces the grout to fill the gaps between the EPBS tail and the surrounding soil. When the grout is in contact with the soil layer, this pressure is transmitted to the surrounding soil. Furthermore, the excessive grouting pressure increases the plastic zone area of the soil and is unfavorable for the EPBS tail sealing (Zhang *et al.* 2021). A slight grouting pressure cannot cause the grout to fill the soil layer (Liu *et al.* 2020, Liu *et al.* 2021, Zhang *et al.* 2017, Jiang *et al.* 2021); hence, a theoretically reasonable grouting pressure that can enable the grout to fill the surrounding soil without any plastic soil damage was estimated. The grout pressure is calculated as follows

$$\sigma_{opt} = \sqrt{\left[\left(H\gamma\tan^2(45°-\frac{\varphi}{2})-2c\tan(45°-\frac{\varphi}{2})\right]\cdot\left[\left(H\gamma\tan^2(45°-\frac{\varphi}{2})+2c\tan(45°-\frac{\varphi}{2})\right]\right.}, \quad (1)$$

$$\sigma_a = \sigma_{opt}+\Delta\sigma, \quad (2)$$

where σ_{opt} is the optimal grouting pressure, σ_a is the actual grouting pressure, $\Delta\sigma$ is the pressure loss in the pipeline, H is the depth of the tunnel center, and γ, c, and φ are the weighted average parameter values of the tunnel crossing strata and the overlying soil (see Table 1).

According to Eqs. (1) and (2), σ_{opt}=188.25 kPa could be calculated. Considering that the pressure loss of the grout along the grouting pipeline is about 30 kPa, the grouting pressure σ_a is about 220 kPa.

2.2.2 Calculation of reasonable grouting quantity

When calculating the theoretical grouting quantity, it is assumed that the soil around the shield uniformly converges, and the grout can fill the gap. The actual grouting volume is always greater than the theoretical value. The grouting volume is calculated as shown in Eqs. (3) and (4)

$$V_t = 0.25\cdot\pi\cdot(D_e^2-D^2), \quad (3)$$

$$V_a = \alpha\cdot V_t, \quad (4)$$

where V_t is the theoretical grouting volume, V_a is the actual grouting volume, α is the grouting quantity ratio, D_e is the diameter of the shield excavation, and D is the outer diameter of the tunnel.

During shield tunneling, the convergence of the soil around the shield is uneven, and the gap formed at the tail of the shield is not a concentric ring. In the construction, the shield tail-grouting usually cannot fill the gap completely; therefore, soil loss at the shield tail still exists. A simplified calculation of the gap parameters is presented in Fig. 4 and listed as below

$$V_l = 0.25\cdot\pi\cdot(D_e^2-D^2)- V_a, \quad (5)$$

$$V_l = 0.25\cdot\pi\cdot D_e^2-0.25\cdot\pi\cdot(D_e-g)^2, \quad (6)$$

$$V_l = \eta\cdot 0.25\cdot\pi\cdot D^2, \quad (7)$$

Table 2 Parameters of grout

Item	Performance parameter					
Composition /(kg/m^3)	Cement	Fly ash	Bentonite	Sand	Additives	Water
	220	350	180	250	0.22	132
T_i/h	5					
Fluidity /cm	8–12					
Bleeding ratio	<5%					
$E_{(t)}$/MPa	24 h				28 d	
	150				250	

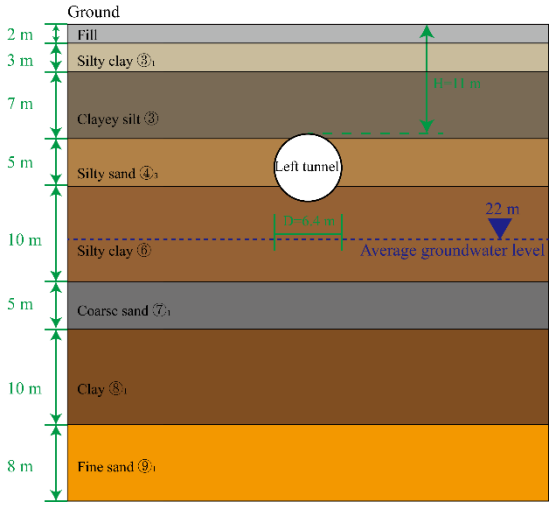

Fig. 3 Sectional view of the soil layer

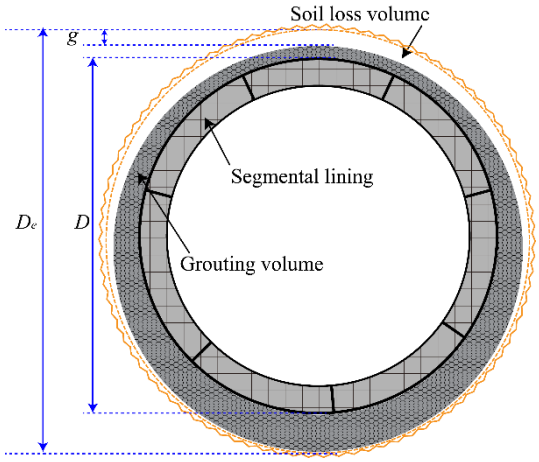

Fig. 4 Non-uniform distribution of shield tail gap

where g is the gap parameter of the shield tail, V_l is the stratum loss volume, and η is the stratum volume loss ratio. From Eqs. (5)-(7), we obtain

$$V_a = 0.25\cdot\pi\cdot(D_e^2-(1+\eta)\cdot D^2), \tag{8}$$

$$g = D_e-\sqrt{D_e^2-\eta D^2}. \tag{9}$$

The stratum volume loss in the shield tunneling process can be divided into four components: (a) volume loss at the shield excavation face, $V_{l,f}$; (b) volume loss along with the shield shell, $V_{l,s}$; (c) volume loss at the shield tail, $V_{l,t}$; and (d) volume loss after the shield tail passes, $V_{l,c}$ (Cheng *et al.* 2019). Corresponding to these four parts of the soil volume loss are the soil volume ratios, η_f, η_s, η_t, and η_c.

$$V_l = V_{l,f} + V_{l,s} + V_{l,t}+V_{l,c} \tag{10}$$

$$\eta = \eta_f+\eta_s+\eta_t+\eta_c \tag{11}$$

The parameters of the settlement trough can be obtained through a Gaussian fitting of the settlement data. The formula is as follows (Peck 1969)

$$S_{(x)} = S_{max}\cdot\exp[-x^2/(2i^2)], \tag{12}$$

$$\eta = \frac{4\sqrt{2\pi}S_{max}\cdot i}{\pi D^2}, \tag{13}$$

where $S_{(x)}$ is the settlement at position x on the ground surface, S_{max} is the maximum settlement value of the settlement trough, which is located on the symmetric center of the settlement curve, x is the distance from the center of the settlement curve to the calculation point, and i is the width of the settlement trough, that is, the distance from the center to the inflection point of the settlement curve.

2.2.3 Hardening characteristics of cement slurry

The grout used in construction was tested, and the proportion, stone rate, condensation parameters, and strength of the grout were analyzed. The performance indices of the grout are listed in Table 2.

2.3 Test methodologies

The left tunnel of the 1606th–1655th ring at the newly added station area was selected as the test field. During the shield tunneling, if the tail-grouting ratio α = 0, it may induce large-scale ground settlement or even stratum collapse, endangering the safety of the ground and surrounding buildings. Therefore, field tests to reduce the grouting quantity usually cannot be implemented. However, in this project, the soil and tunnel segments could eventually be removed, and the surrounding

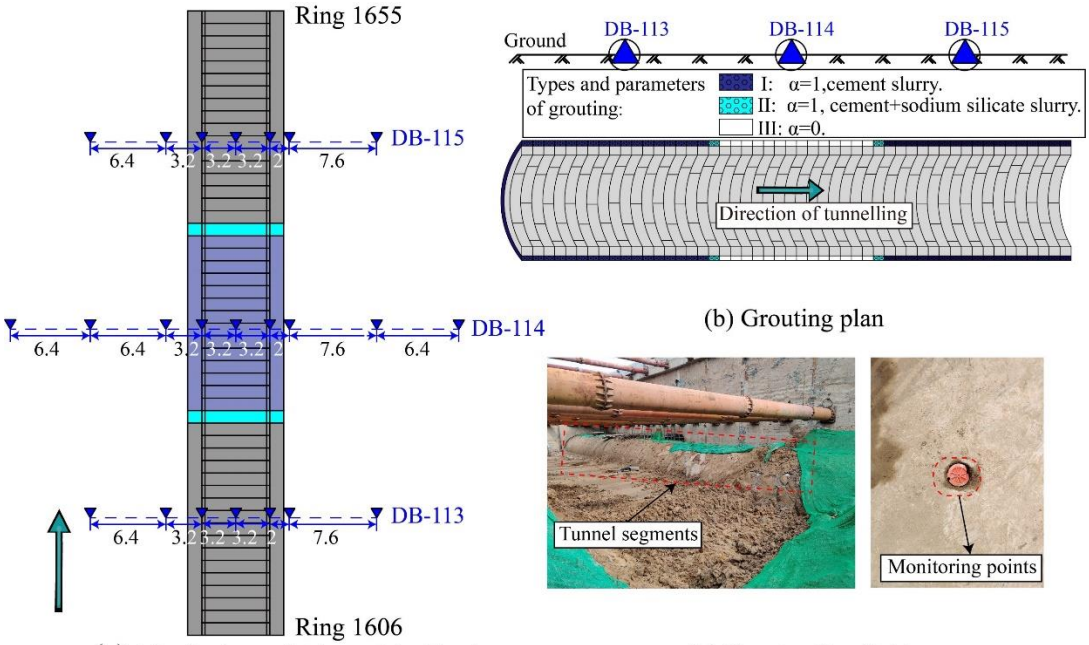

Fig. 5 Layout plan of monitoring points

ground was empty; hence, it was possible to perform field tests. The grouting quantity ratio was set to 100% when the 1606th–1624th ring of the left tunnel was excavated; it was set to 0 when the 1624th–1637th ring was tunneled, and was restored to 100% at the 1637th–1655th ring. Cement and sodium silicate ($Na_2O{\cdot}nSiO_2$) were applied in the 1623rd and 1637th rings for tail-grouting. The setting time of this two-liquid slurry was 7 s, which could prevent the slurry from flowing back to the non-grouting area (Kim and Park 2017, Shah *et al.* 2018). The ground settlement monitoring data were recorded during the field test; the layout of the monitoring points is shown in Fig. 5.

3. Test results

3.1 Surface settlements

The settlement values of the three monitoring faces are shown in Figs. 6(a)-6(c). It can be seen that the evolution of the settlement curves of DB-113 and DB-115 are the same, and the final shape is similar to a "V" shape. Conversely, the final settlement curve of the monitoring surface DB-114 is in a "U" shape, and its evolution law is slightly different. The initial settlement ratio of the surface measurement point above the tunnel edge is significantly faster than that above the tunnel axis. However, the ultimate maximum settlement is still at the center of the surface.

Fig. 6(d) shows the settlement curve of the center point of the ground surface during shield tunneling. The settlement curve can be divided into four stages based on the distance between the shield excavation face and the position of the monitoring points.

Stage I: Before the cutterhead reaches the monitoring surface.

Stage II: The cutterhead passes, and the shield tail does not leave the monitoring points.

Stage III: The shield tail is completely separated from the monitoring points until it is 10 m away from them.

Stage IV: The shield tail is more than 10m away from the monitoring points.

As shown in Fig. 6(d), the shield tunneling process mainly causes surface settlement in the second and third stages. The shield passes through the tunneling section with a grouting ratio of 0 before reaching the monitoring face DB-115. Furthermore, compared to the curve phase of DB-113, that of BD-115 starts to decline earlier in the first stage; the total settlement was also slightly larger. The curve of DB-114 falls rapidly from the second stage onward, and the third stage accounts for the highest amount of settlement.

3.2 Calculation of volume loss and gap parameters

A Gaussian fitting was performed on the monitoring data. And the soil loss parameter η can be calculated from the Gaussian fit results of the monitoring data combine with Eq. (13). And then, the shield tail gap parameter g could be calculated using Eq. (10). Table 3 lists the calculation and fitting processes. Eqs. (10) and (11) divide the process of shield passing through the monitoring surface into four stages and define the soil volume loss parameters of each stage. By analyzing the data recorded at the measurement points during the shield passing through the monitoring surface and dividing the settlement curve into four stages accordingly (as shown in Fig. 6(d)), the ground loss parameters of each stage and their percentages can be obtained. As shown in Fig. 7, the soil volume loss ratio η_s along with the shield shell and the soil volume loss η_t at the shield tail account for the most significant proportion. The monitoring surfaces DB-113 and DB-115 are similar; the

Table 3 Soil volume loss for three monitoring sections

Monitoring sections	Fitting			η_f	η_s	η_t	η_c	η	g
	S_{max}/mm	i/m	R-square	%	%	%	%	%	mm
DB-113	26.1	3.68	0.96953	0.22	0.65	0.40	0.06	1.33	40.9
DB-114	160.9	7.15	0.99467	0.47	5.36	9.88	0.20	15.91	510.0
DB-115	34.2	4.01	0.98456	0.10	1.16	0.50	0.14	1.90	58.6

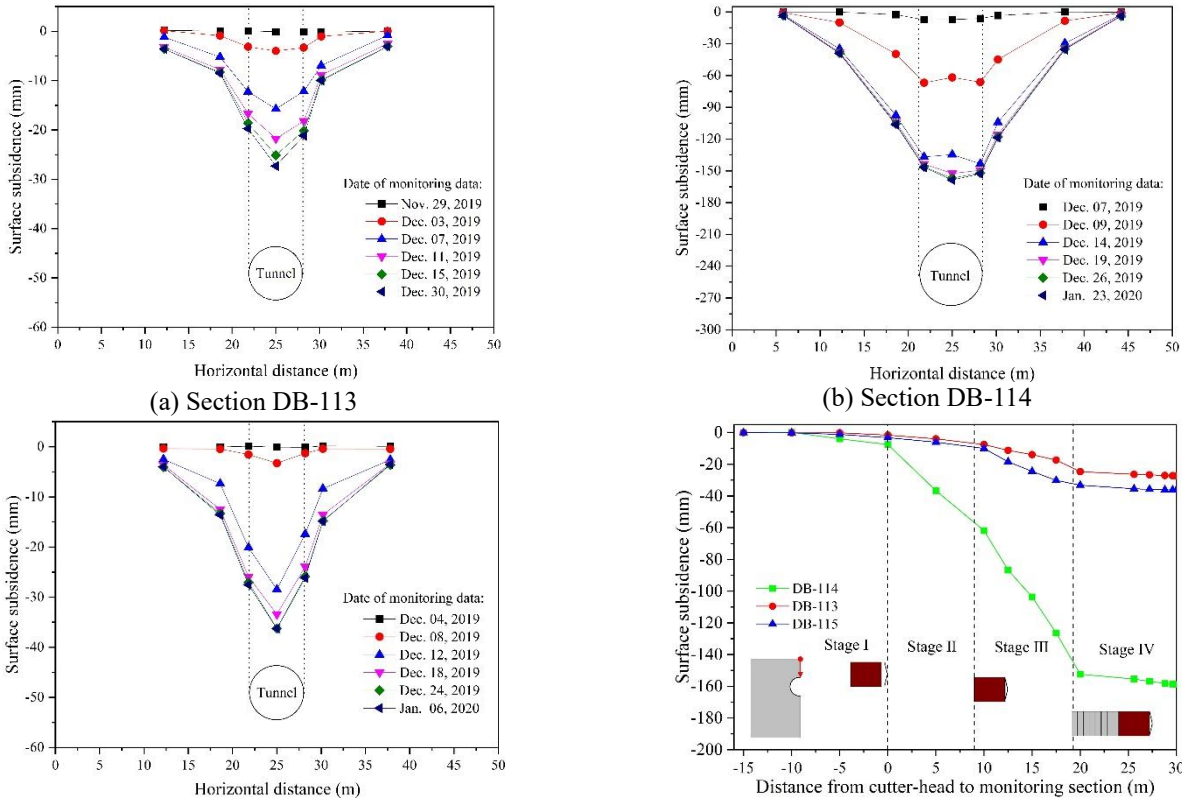

(a) Section DB-113 (b) Section DB-114

(c) Section DB-115 (d) Time-settlement curve

Fig. 6 Surface subsidence data of monitoring

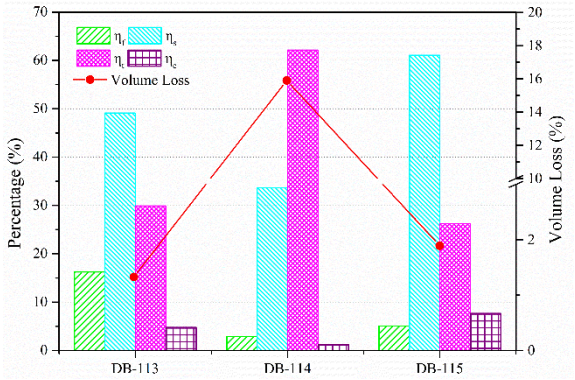

Fig. 7 Percentage of four components of soil volume loss for three monitoring sections

proportion of η_s is higher than that of η_t, but on the monitoring surface DB-114 with the grouting ratio $\alpha = 0$, the proportion of η_t is much higher than that of η_s. This is because the gap at the shield tail under the monitoring surface DB-114 is not sufficiently filled. The value of the shield tail gap parameter g can better explain this phenomenon directly. It is calculated based on the non-uniform convergence law of the shield tail gap assumed in Fig. 4 and Eqs. (3)-(9). Based on the monitoring data of the three monitoring surfaces, the calculated shield tail gap parameters g are 40.9 mm, 510.0 mm, and 58.6 mm, respectively. Because the cracks in the soil and the penetration of the grout in the cracks are irregular, the size of parameter g may not be the actual value of the shield tail gap. However, it is reasonable to use the value of g to reflect the relative size of the shield tail gap. The gap parameter value of the monitoring surface DB-114 is much larger than that of the other two monitoring surfaces—a quantitative manifestation of the difference in the surface settlements caused by the grouting ratio $\alpha = 0$ and $\alpha = 1$.

4. Three-dimensional numerical model

4.1 Three-dimensional numerical model for shield tunneling

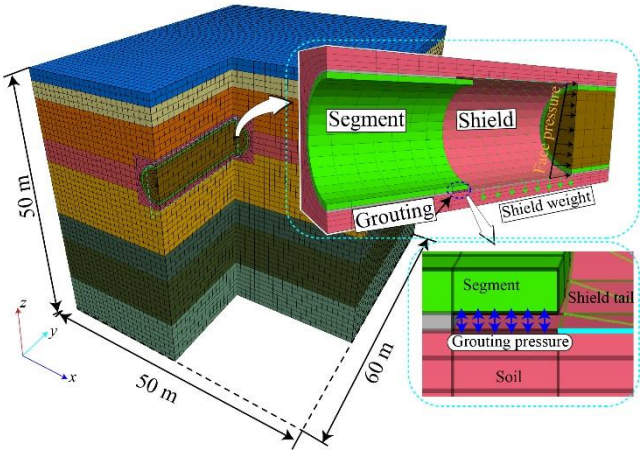

(a) Three-dimensional model of shield tunneling

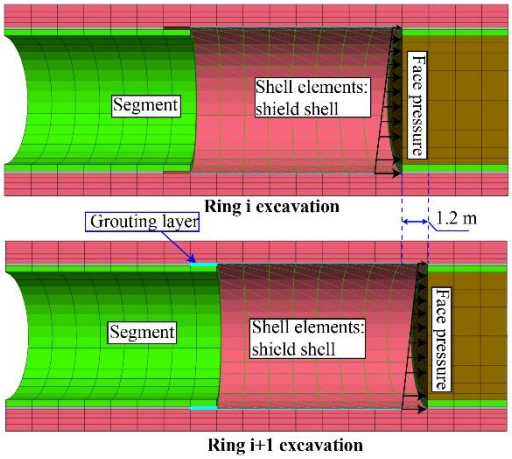

(b) Schematic diagram of shield step-by-step tunneling

Fig. 8 Three-dimensional model and tunneling process of shield tunnel

To obtain more laws between the grouting parameters and surface settlement, this study also employed numerical simulation methods for research based on the field tests. A three-dimensional finite-difference grid was established using the FLAC^{3D} software, as shown in Fig. 8(a). The figure indicates the global coordinate direction of the model. The size of the model is 50 m×60 m×50 m ($x \times y \times z$), which is sufficiently large to avoid the influence of the boundary effects (Mroueh and Shahrour 2008, Zhao *et al.* 2015). The limit displacement boundary conditions of the model were set as follows: 1) x-direction: $x = 0$, 50 boundaries; 2) y-direction: $y = 0$, 60 boundaries; 3) z-direction: $z = 0$ boundary. The top boundary, $z = 50$, was the free surface.

4.2 Simulation of different phases of the shield tunneling process

Shield tunneling is a construction activity consisting of several continuous processes, including shield advancement, soil excavation, segment assembly, and tail-grouting. However, in recent studies, a simplified step-by-step excavation sequence is typically used to simulate the shield tunneling process (Kasper and Meschke 2006, Mroueh and Shahrour 2008, Swoboda *et al.* 2004). The length of each excavation cycle is the width of the ring segment (1.2 m). A schematic of the excavation process is shown in Fig. 8(b). In this numerical simulation, the grout behavior, weight of the shield, construction load, excavation face pressure, and segment lining were considered. The excavation steps are as follows:

(1) Excavate the soil within 1.2 m behind the tunnel face and apply support pressure to the excavation face to maintain the stability of the soil;

(2) Apply a grouting pressure and install a ring of segments behind the shield tail;

(3) After the excavation calculation is stable, proceed to the subsequent ring excavation.

Table 4 Tunnel segmental lining parameters

Structure	E(GPa)	ν	ρ(kg·m^{-3})
Segment	36.0	0.2	2500
Shield shell	200	0.25	8000

Note: E = Young's modulus; ρ = Density; ν = Poisson's ratio.

4.3 Material constitutive model and parameters

4.3.1 Material parameters

The tunnel mainly passes through silt—specifically, a silty sand stratum. According to previous studies, the Mohr–Coulomb strength criterion can accurately reflect the elastoplastic stress state of this type of soil. Moreover, the parameters required by the Mohr–Coulomb constitutive relationship can easily be obtained experimentally (Lv *et al.* 2020; Rezaei and Ahmadi-adli 2020). The saturation gravity γ_{sat}, Poisson's ratio ν, Young's modulus E, cohesion c, and friction angle φ of each soil layer are listed in Table 1.

In addition to the soil, the following materials were used in the numerical simulation: shield shell, concrete segment, and cement grout. Therefore, the following constitutive models and structures were also used: (a) Null model: used for materials that have been excavated, (b) Isotropic elastic model: used for concrete segments and hardened slurry, and (c) Shell element: used for steel shield shell. The parameters of the materials are listed in Table 4.

4.3.2 Face pressure

The support pressure of the excavation face can be calculated using Eq. (14)

$$\sigma_{f,z} = K_0 \cdot \sigma_{zz} + \sigma_t, \tag{14}$$

where $\sigma_{f,z}$ is the supporting stress at the depth of the excavation surface at z (the bottom of the model corresponds to z=0, and the top of the model corresponds to z=50), K_0 is the lateral earth pressure coefficient of the soil at rest, σ_{zz} is the vertical stress at a depth of z, and σ_t is the additional stress, which can be taken as σ_t =20 kPa. The supporting force is the trapezoidal stress (as shown in Fig. 8(b)), and the expression of this stress is

$$\sigma_{f,z} = \sigma_{f,0} + g_0 \cdot z, \tag{15}$$

In the formula, σ_0 = -71.18 kPa, and g_0 is the stress gradient 4.5 kPa/m.

4.3.3 Tail-grouting

The numerical simulation of the tail-grouting behavior can be realized through using three parameters: the grouting quantity, grouting pressure, and grouting strength.

(1) Grouting pressure: In the numerical simulation, the grouting pressure can be simplified to a uniform load. The calculation of the grouting pressure is given in Eqs. (1) and (2) in Section 2.2.1.

(2) Young's modulus of grout: The strength of the grout is usually not a fixed value because the strength of the grout proportionally increases with the time after grout injection. The time-varying Young's modulus $E_{(t)}$ and time-varying Poisson's ratio $\nu_{(t)}$ have often been used to simulate the hardening process of the grout (Lambrughi *et al*. 2012, Meschke 1996, Meschke *et al*. 1996). The slurry hardening law used in this study is given by Eq. (16) and Fig. 9(a).

(3) Grouting quantity: As shown in Eqs. (3) and (4), when the actual grouting quantity is less than the theoretical grouting quantity (α<1), there is a gap in the shield tail (as shown in Fig. 10(a); as can be seen, there is an unfilled gap above the construction gap). In the continuum numerical simulation program such as FLAC^{3D}, the method of reflecting the insufficient filling in the construction gap is usually equivalently replaced by reducing the material strength. After grouting, the construction gap layer is regarded as a uniform material with a specific strength (a substitute layer such as grout), and its strength can be reduced according to the air content. Based on the strength reduction algorithm of the concrete air-entraining agent, once the air content increases by 1%, the strength of the equivalent layer decreases by 4% (Han *et al*. 2021, Oreste *et al*. 2021, Hunan *et al*. 2011). The grouting parameters and the final strength of the grout are shown in Eq. (17) and Fig. 9(b).

$$E_t = \begin{cases} E_i & t=0 \\ E_g\left[1-\exp\left(-0.2\left(\frac{t}{t_0}\right)\right)\right] & t\geq t_0 \end{cases}, \quad (16)$$

$$E_{(\alpha)} = E_g \cdot 0.96^{(100-100\alpha)}, \quad (17)$$

where E_t is the Young's modulus of the grout at time t, E_g is the Young's modulus of the grout after complete hardening, t is the injection time of the grout, t_0 denote the initial hardening time of the grout, E_i is the initial value of the Young's modulus of the grout, and $E_{(\alpha)}$ is the final strength of the grout under different grouting parameters.

The FDM calculation procedure seems difficult to be applied directly in the case of a grouting ratio greater than 1. Therefore, the idea of equivalent replacement is needed to simulate the mechanical behavior of the grouted layer. As shown in Fig. 10(b), a homogeneous material is assumed to replace the grouted zone at the shield tail after grouting, and this "grout-soil" mix is used to equivalently replace the role of the grout. The "grout-soil" mixed layer has a certain thickness, which can be calculated by the following equation

$$\Delta w = w_s \cdot \sqrt{\alpha}, \quad (18)$$

$$w_s = 0.5 \cdot (D_e - D), \quad (19)$$

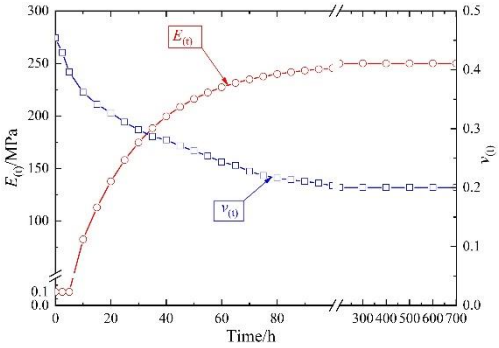

(a) Time-dependent Young's modulus and Poisson's ratio of the tail void grout

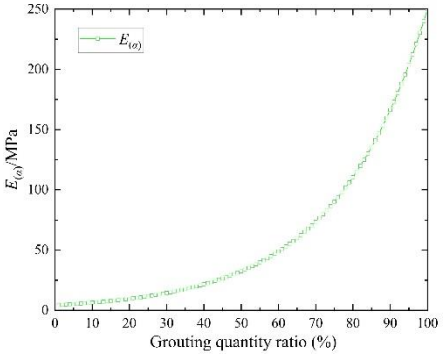

(b) Final strength of the tail-grouting layer under different grouting quantity ratios

Fig. 9 Grout strength parameters in numerical calculation

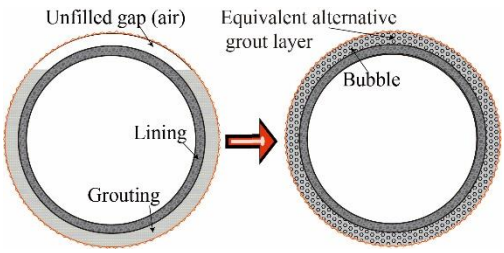

(a) Simplified diagram of construction gap-filling when α<1

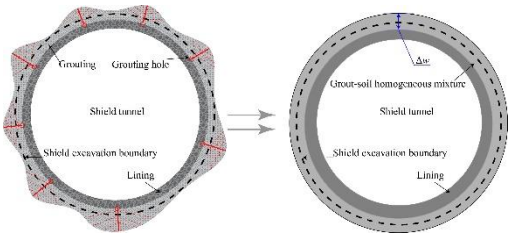

(b) Simplified diagram of the "grout-soil" mixed layer when α>1

Fig. 10 Equivalent grouting layer in numerical calculation

where Δw is the average thickness of the "grout-soil mixed" layer, w_s denote the shield excavation gap, and D_e and D are defined in Eqs. (4) and (5).

4.3.4 Interface

The tunnel segment is a circular material made of reinforced concrete, which is assumed to be an anisotropic elastomer with high strength in the numerical calculations.

Table 5 Parameters of the interface

Interface	Bonded-slip	*k*s	*k*n	*c*	*φ*
		kPa	MPa	Pa	°
value	on	100	200	0	15

Note: *k*s, *k*n are shear stiffness and normal stiffness, respectively

During the construction process, two adjacent segments were connected by bolts. However, the strength of the bolts is usually not considered in the design calculation; hence, the adjacent segments are allowed shearing dislocation in the calculation (Chen *et al*. 2020, Sjölander *et al*. 2020). The contact strength of the segments cannot be calculated based on the strength of the segments because the contact between the segment rings is not rigid. As shown in Fig. 11, the interface can simulate the contact characteristics. The interface parameters are listed in Table 5. For the contact surface, this model assumes the following:

(a) The contact surface of the adjacent segments has no tensile strength. That is, the strength of the bolt connection between the rings is not considered.

(b) Contact surface has high compressive strength. That is, the joints of the segments are not damaged during compression.

(c) The contact surface of adjacent segments has a specific shear strength and frictional angle.

4.4 Verification of the numerical model

After determining the numerical calculation model and material parameters, the accuracy of the model needs to be verified. The reliability of the model can be verified by analyzing the development law of the surface deformation during tunnel excavation and the final settlement curve. Figs. 13(b) and 12(a) respectively compare the consistency of the settlement curve of the numerical simulation during and after the tunnel excavation with the field test monitoring data. As seen from the figures, the numerical calculation results are consistent with the monitoring data and, thus, the model is correct.

5. Numerical results

5.1 Influence of different grouting quantities

The numerical simulation surface settlement curves of different tail-grouting quantity ratios are shown in Fig. 12(a) and are compared with the measured data of DB-113 and DB-114. The calculated results are consistent with the monitored data. The Gaussian fits the five curves, and the calculation process is presented in Table 6. Fig. 12(b) shows the relationship between the soil volume loss η, gap parameter g, maximum settlement S_{max}, and the grouting quantity ratio α. The linear fitting expression can accurately predict the changing trend of the data.

The reasonable grouting effect appears when the surface deformation is 0 (Li 2020), which indicates the optimal grouting quantity. In the numerical simulation part of this

Table 6 Gap parameters for different grouting quantities

α(%)	Fitting			η	g
	S_{max}/mm	*i*/m	R^2	%	mm
100	32.54	6.62	0.998	1.68	52.2
75	73.80	6.92	0.999	3 .98	124.1
50	112.55	8.57	0.999	7.52	236.0
25	136.73	9.67	0.999	10.31	326.1
0	169.98	11.39	0.999	15.09	483.1

Note: R^2 is the goodness of fit, and its value is approximately 1, indicating a better fit

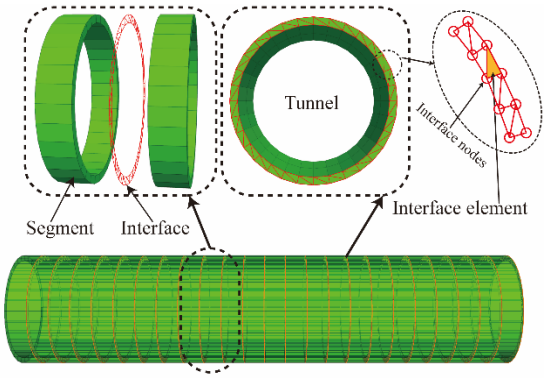

Fig. 11 Interface between adjacent segments

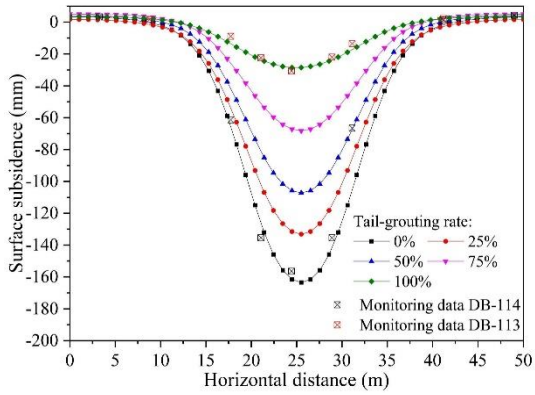

(a) Surface settlement curves of different grouting quantities

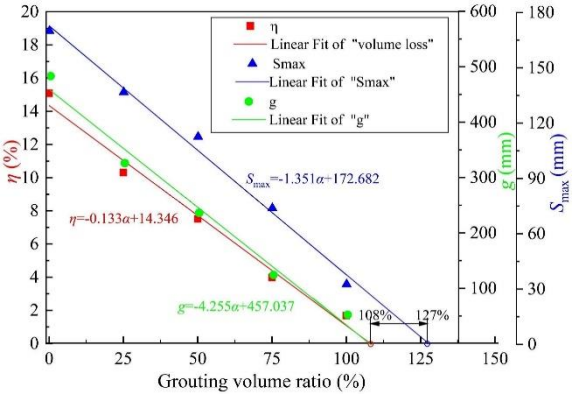

(b) Linear fitting of η, g, S_{max} to α

Fig. 12 Numerical calculation of horizontal surface settlement

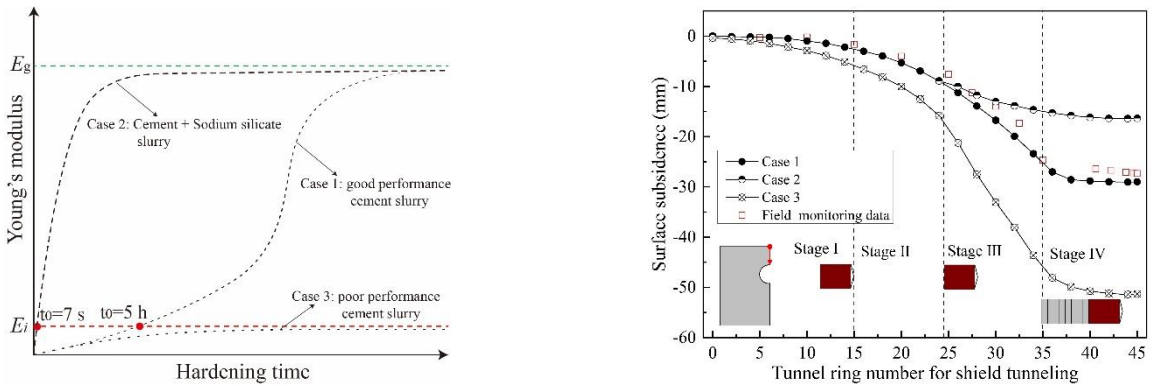

(a) Different hardening types of grout (b) Settlement at the center of the surface

Fig. 13 Evolution of the surface settlement under different hardening types of grout

study, the relationship between the grouting volume and related parameters such as the soil volume loss ratio η, gap parameter g, and the maximum settlement amount S_{max} are mainly analyzed. Thus, the optimal grouting quantity ratio is obtained according to the rationality of the three parameters and determined as 1.08 to 1.27.

5.2 Influence of different hardening types of cement grouting

The setting time of the tail-grouting slurry affects the development law of the formation or deformation. In the Beijing area, the performance standard of cement grout in shield engineering is defined in the construction specification "GB/T 50310-2018". Table 2 lists one of the most commonly used synchronous grouting material formulas in this area. In this numerical test, three kinds of grout with different hardening properties were selected, as shown in Fig. 13(a). The strength of the cement grout with good performance reaches the initial strength E_i after 5–8 h and gains the final strength E_g after a long time (Case 1). However, the poor performance of the cement slurry does not reach the initial strength E_i until it sets for a long time (Case 3). In addition, the double liquid slurry (cement and sodium silicate) is often used in projects with significant risks. The hardening time of this slurry is rapid, usually reaching the initial strength E_i in 5–30 s and then reaching the final strength E_g relatively quickly (Case 2). This study investigated the influence of different grout condensation forms on the development of the surface settlement by simulating different grout-hardening processes. The grout performance of Case 1 was consistent with that used in the actual construction. As shown in Fig. 13(b), the law of the central surface settlement of Case 1 was consistent with the monitoring data.

Compared with Case 2, the deformation curve of Case 1 is more consistent at Stages I and II. The hardening time of the slurry has little effect on the surface settlement before the shield tail is passed. When the shield tail passes through, the rapidly condensing slurry has an apparent inhibitory effect on increasing the surface settlement and making the development ratio of the surface settlement slow and that of the final settlement small.

In Case 3, the development law of the surface settlement is different; the settlement curve shows a more significant increment and slopes from the beginning. Especially in Stage III, the slowly hardening slurry makes it challenging to control the development of the surface settlement using the tail-grouting, which seriously affects the engineering qualities.

5.3 Range of disturbed strata

Figs. 14(a)-14(e) show the three-dimensional surface settlement caused by the shield tunneling under five different grouting quantity ratios. As the grouting ratio decreases, both the disturbance range and maximum surface settlement increase. Under normal construction conditions (α = 1), the surface forms a "trench" of equal width after shield tunneling. The transverse section of the "trench" is a standard settlement curve conforming to the Gaussian distribution; when the grouting ratio α is less than "1," the center of the surface settlement "trench" gradually develops downward. The transverse section of the surface settlement is a Gaussian curve (Fig. 12(a)); the longitudinal section curve still complies with the Gaussian distribution (as shown in Fig. 15(a)). Therefore, when α<1, the laws of the surface subsidence in the horizontal (x) and vertical (y) directions follow a Gaussian distribution. We can use the parameter of the width of the settlement trough i to reflect the range of the disturbed stratum. As shown in Fig. 15(b), for every 10% increase in the grouting ratio α, the width of the lateral settlement trough decreases by 0.49 m, and the width of the longitudinal settlement trough decreases by 0.45 m. The horizontal and vertical settlement curves of the ground surface are given by Eq. (20)

$$\begin{cases} S_{(x)} = S_{max} \cdot \exp(-x^2/2i_x^2) \\ S_{(y)} = S_{max} \cdot \exp(-y^2/2i_y^2) \end{cases}, \tag{20}$$

where $S_{(x)}$ and $S_{(y)}$ are the settlement values of the ground along the x- and y-directions, respectively, and i_x and i_y are the widths of the settlement troughs along the x- and y-directions, respectively.

The relationship between the width of the settlement trough in the x- and y-directions with the grouting quantity ratio is shown in Fig. 15(b). i_x and i_y have the following relationship

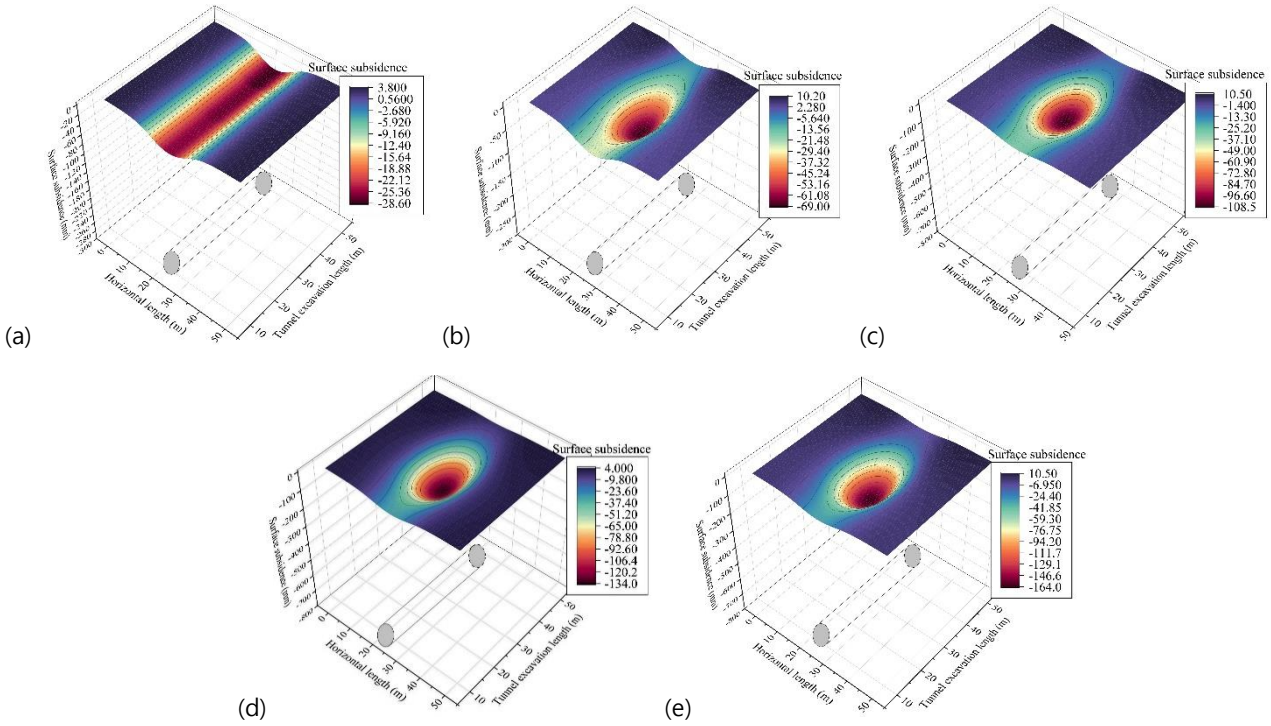

Fig. 14 Three-dimensional surface settlement contours with synchronous grouting parameters: (a) $\alpha = 1$, (b) $\alpha = 0.75$, (c) $\alpha = 0.5$, (d) $\alpha = 0.25$, and (e) $\alpha = 0$

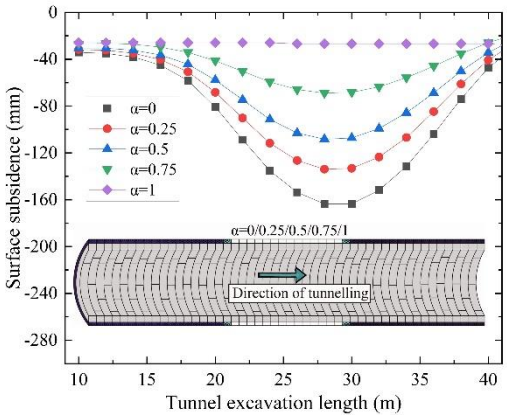

(a) Longitudinal surface settlement curve

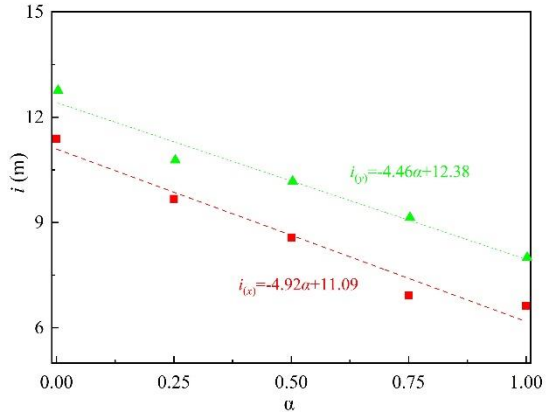

(b) Linear relationship between i and α

Fig. 15 Numerical calculation of longitudinal surface settlement

$$i_x = 0.89 i_y + 2.50, \tag{21}$$

$$i = H \cdot K, \tag{22}$$

$$K = i/H = \pi D^2 \eta / 4\sqrt{2\pi} H S_{\max}, \tag{23}$$

In the formula, K is the width coefficient of the settlement trough. The width coefficient K_x of the horizontal settlement trough lies within the 0.6–1.0 range; the width coefficient K_y of the longitudinal settlement trough is within the 0.7–1.2 range.

Surface subsidence is induced by both the soil volume loss and the soil consolidation. When $\alpha = 1$, the volume loss ratio is only 1.68%, and when α increases to 1.08, the volume loss ratio can be reduced to 0. Soil consolidation causes almost all surface deformations; therefore, increasing the grouting quantity ratio can reduce the soil volume loss caused by shield tunneling.

5.4 Stress state of ground and tunnel lining

Owing to the disturbance and volume loss caused by the shield excavation, the vertical stress above the tunnel decreases, resulting in a loose zone in the soil. The tail-grouting pressure has a stress compensation effect on the soil layer around the tunnel and can restrain some strata deformation. Therefore, it is difficult to achieve satisfactory results when the grouting pressure or the grouting quantity is insufficient. Figs. 16(a)-16(e) show the vertical stress distribution in the stratum under five groups of different

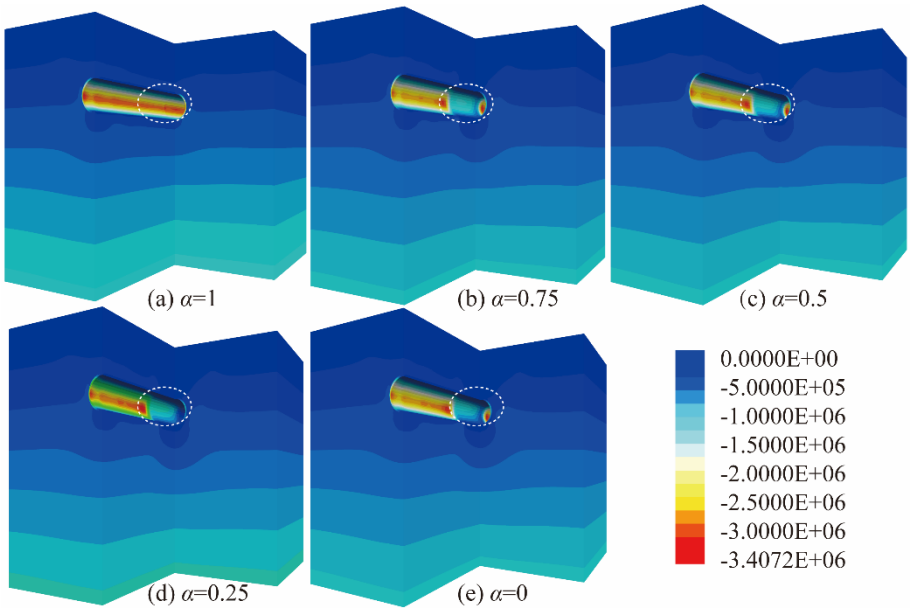

Fig. 16 Vertical stress of the model (unit: Pa)

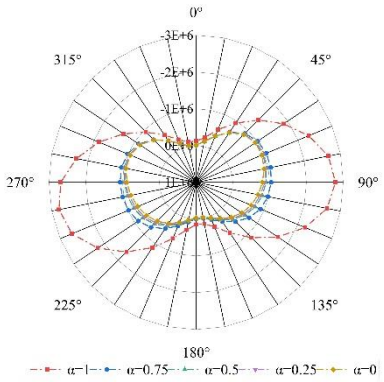

(a) Stress (unit: Pa)

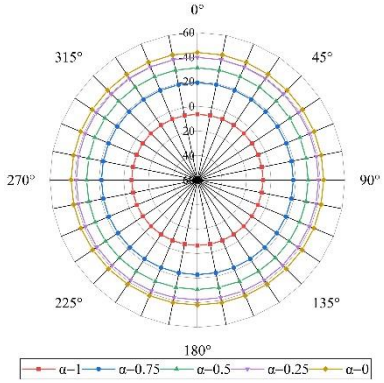

(b) Deformation (unit: mm)

Fig. 17 Tunnel state under different grouting quantities

grouting quantities. With a decrease in the synchronous grouting amount, the loosened zone above the tunnel gradually expands, and the stress in the stratum changes significantly.

The most apparent feature in the figure is the difference in the resistances of the surrounding soil of the tunnel support structure with different grouting quantities. When the grouting amount is sufficient (α = 1), the stress state of the tunnel segments in each section is consistent. Conversely, when the grouting quantity ratio α<1, the stress state of the tunnel segments in the inadequate grouting section is significantly different from that of the segments before and after the grouting. Without sufficient grouting quantity, the tunnel segments are no longer compressed closely by the surrounding soil layer, and the lateral pressure on the segments is significantly reduced. As shown in Fig. 17(a), with a decrease in the grouting quantity ratio, the stress reduction of the tunnel segments gradually increases, resulting in the deformation of the segments. The deformations of the tunnel segments under different grouting quantities are shown in Fig. 17(b). When the grouting quantity is sufficient (α = 1), the unloading effect of the soil after the tunnel excavation causes the segments to move upward by approximately 6 mm. Conversely, when it is insufficient (α<1), the segments lack the support of the grout after it protrudes from the shield tail and, thus, deforms downward. The smaller grouting quantity ratio results in a greater deformation.

6. Conclusions

In this study, field tests and numerical simulations were combined to investigate the effect of shield tail-grouting parameters on surface settlement. The following conclusions can be drawn.

- The field tests data of the shield tunneling with different grouting quantities showed that the surface settlement troughs were "V" shaped when the grouting quantity ratio was 1 and "U" shaped when the grouting quantity ratio was less than 1. The extreme values of the settlement appeared directly above the tunnel axis. However, there were apparent differences in the evolution processes of the settlement trough: when the grouting quantity ratio was 0, the initial settlement ratio on the left and right walls of the tunnel was faster than that above the axis. Conversely, when it was 1, the settlement at the axial center was the fastest.

- The field test monitoring data show that during shield tunneling, surface subsidence occurred mainly in Stages II and III, and the soil volume loss mainly occurred in these two stages. The grouting quantity affected every stage of the soil volume loss proportion, and the soil losses were the highest in Stage II when the grouting quantity ratio was 1; however, when the grouting ratio was 0, the soil loss ratio was the highest in Stage III.
- The numerical simulation results of five different grouting quantity ratios indicate that the soil volume loss ratio η, parameter g of the shield tail gap, and maximum settlement S_{max} are linearly related to the grouting quantity ratios. Based on this linear relationship, an evaluation method for the optimal grouting amount was formulated, and the recommended grouting quantity ratio was within the 1.08–1.27 range, which could provide a reference for similar projects.
- The different hardening characteristics of the grout greatly influence the development law of the surface settlement. The grout with the feature of quick-setting and great strength could effectively restrain the increase in the surface settlement when the shield tail was out of the segment.
- Through the analysis of the three-dimensional displacement of the ground surface, it could be seen that when the grouting ratio α<1, the horizontal and vertical settlement curves of the ground conform to the Gaussian distribution, and there was a linear correlation between the width i_x of the horizontal settlement trough and the width i_y of the longitudinal settlement trough. Under this geological condition, for every 10% increase in the grouting quantity ratio, the width of the transverse settlement trough decreased by 0.49 m and that of the longitudinal settlement trough decreased by 0.45 m. The width coefficients of the transverse and longitudinal settlement troughs were K_x = 0.6–1.0 and K_y = 0.7–1.2, respectively. The soil volume loss caused by insufficient grouting was the leading cause of the ground surface settlement.
- The stress results obtained by the numerical simulation showed that with a decrease in the grouting quantity ratio, the loosening of the ground above the tunnel expanded, and the soil deformation was more likely to be transmitted to the ground surface, which in turn caused a more significant ground deformation. Moreover, the amount of stress reduction in the tunnel segments gradually decreased. When the grouting was insufficient (α<1), owing to the lack of grout support, the segment was deformed downward after being removed from the shield tail.

During the field test in this study, we conducted two sets of shield tunneling tests with grouting quantity ratios α = 1 and α = 0. However, owing to the limitations of the construction period, it was impossible to conduct more shield tunneling tests with different grouting ratios. Therefore, based on the field test, this study adopted a numerical simulation to study the influence of the grouting parameters on the surface settlements, which can provide a reference for the selection and control of tail-grouting parameters in shield engineering.

Acknowledgments

This study was financially supported by the National Natural Science Foundation of China (Grant No. U1261212). The first and corresponding authors would also like to acknowledge the support provided by the China Railway 12th Bureau Group.

References

Chen, R., Chen, S., Wu, H., Liu, Y. and Meng, F. (2020), "Investigation on deformation behavior and failure mechanism of a segmental ring in shield tunnels based on elaborate numerical simulation", *Eng. Fail. Anal.*, **117**, 104960. https://doi.org/10.1016/j.engfailanal.2020.104960.

Cheng, H., Chen, J. and Chen, G. (2019), "Analysis of ground surface settlement induced by a large EPB shield tunnelling: a case study in Beijing, China", *Environ. Earth Sci.*, **78**(20), 1-18. https://doi.org/10.1007/s12665-019-8620-6.

Ding, W., Duan, C., Zhu, Y., Zhao, T., Huang, D. and Li, P. (2019), "The behavior of synchronous grouting in a quasi-rectangular shield tunnel based on a large visualized model test", *Tunn. Undergr. Sp. Tech.*, **83**, 409-424. https://doi.org/10.1016/j.tust.2018.10.006.

Do, N.A., Dias, D., Oreste, P. and Irini, D.M. (2014), "Three-dimensional numerical simulation for mechanized tunnelling in soft ground: the influence of the joint pattern", *Acta Geotech.*, **9**(4), 673-694. https://doi.org/10.1007/s11440-013-0279-7.

Han, C., Wei, J., Zhang, W., Zhou, W., Yin, H., Xie, D., Yang, F., Li, X. and Man, X. (2021), "Numerical investigation of grout diffusion accounting for the dynamic pressure boundary condition and spatiotemporal variation in slurry viscosity", *Int. J. Geomech.*, **21**(4), 04021018. https://orcid.org/10.1061/(ASCE)GM.1943-5622.0001945.

Hunan, U., Tianjin, U., Tongji, U. and Southeast, U., (2011), "Architecture Material", *China Architecture & Building Press*.

Jiang, H., Cheng, J.G., Zhang J.X., Zhang, J.L., Su, Y.R. and Zheng Y.F. (2021), "Principle and application of in-situ monitoring system for ground displacement induced by shield tunnelling", *Tunn. Undergr. Sp. Tech.*, **112**(13-20), 103905. https://doi.org/10.1016/j.tust.2021.103905.

Kasper, T. and Meschke, G. (2006), "A numerical study of the effect of soil and grout material properties and cover depth in shield tunnelling", *Comput. Geotech.*, **33**(4-5), 234-247. https://doi.org/10.1016/j.compgeo.2006.04.004.

Kavvadas, M., Litsas, D., Vazaios, I. and Fortsakis, P. (2017), "Development of a 3D finite element model for shield EPB tunnelling", *Tunn. Undergr. Sp. Tech.*, **65**, 22-34. https://doi.org/10.1016/j.tust.2017.02.001.

Kim, D. and Park, K. (2017), "Evaluation of the grouting in the sandy ground using bio injection material", *Geomech. Eng.*, **12**(5), 739-752. https://doi.org/10.12989/gae.2017.12.5.739.

Lambrughi, A., Rodríguez, L.M. and Castellanza, R. (2012), "Development and validation of a 3D numerical model for TBM–EPB mechanised excavations", *Comput. Geotech.*, **40**, 97-113. https://doi.org/10.1016/j.compgeo.2011.10.004.

Lavasan, A.A., Zhao, C., Barciaga, T., Schaufler, A., Steeb, H. and Schanz, T. (2018), "Numerical investigation of tunneling in saturated soil: the role of construction and operation periods", *Acta Geotech.*, **13**(3), 671-691. https://doi.org/10.1007/s11440-017-0595-4.

Li, C. (2020), "Simplified algorithm for grouting pressure and grouting quantity in shield construction", *Int. J. Civ. Eng.*, **18**(4), 419-428. https://doi.org/10.1007/s40999-019-00476-5.

Li, P., Zhang, Q., Zhang, X., Li, S., Li, X. and Zuo, J. (2017), "Grouting diffusion characteristics in faults considering the interaction of multiple grouting", *Int. J. Geomech.*, **17**(5), 04016117. https://orcid.org/10.1061/(ASCE)GM.1943-5622.0000815.

Liu, B., Sang, H., Liu, Q., Kang, Y., Pan, Y., Lu, C. and Zhang, C. (2020), "New algorithm for simulating grout diffusion and migration in fractured rock masses", *Int. J. Geomech.*, **20**(3), 04019188. https://orcid.org/10.1061/(ASCE)GM.1943-5622.0001537.

Liu, B., Sang, H., Liu, Q., Liu, H., Pan, Y. and Kang, Y. (2021), "Laboratory Study on Diffusion and Migration of Grout in Rock Mass Fracture Network", *Int. J. Geomech.*, **21**(1), 04020242. https://orcid.org/10.1061/(ASCE)GM.1943-5622.0001901.

Liu, C., Li, J., Zhang, Z., Li, P., Cui, J., Liu, H. and Yang, Y. (2020), "Model tests on tail-grouting process during URUP shield tunneling in soft soil", *Tunn. Undergr. Sp. Tech.*, **103**, 103451. https://doi.org/10.1016/j.tust.2020.103451.

Lo, K. and Rowe, R. (1982), *Prediction of ground subsidence due to tunnelling in clays*, University of Western Ontario.

Lv, J., Li, X., Li, Z. and Fu, H. (2020), "Numerical simulations of construction of shield tunnel with small clearance to adjacent tunnel without and with isolation pile reinforcement", *KSCE J. Civ. Eng.*, **24**(1), 295-309. https://doi.org/10.1007/s12205-020-1167-y.

Meschke, G. (1996), "Consideration of aging of shotcrete in the context of a 3-D viscoplastic material model", *Int. J. Numer. Meth. Eng.*, **39**(18), 3123-3143.

Meschke, G., Kropik, C. and Mang, H. (1996), "Numerical analyses of tunnel linings by means of a viscoplastic material model for shotcrete", *Int. J. Numer. Meth. Eng.*, **39**(18), 3145-3162.

Mroueh, H. and Shahrour, I. (2008), "A simplified 3D model for tunnel construction using tunnel boring machines", *Tunn. Undergr. Sp. Tech.*, **23**(1), 38-45. https://doi.org/10.1016/j.tust.2006.11.008.

Oreste, P., Sebastiani, D., Spagnoli, G. and Lillis, A. D. (2021), "Analysis of the behavior of the two-component grout around a tunnel segmental lining on the basis of experimental results and analytical approaches", *Transp. Geotech.*, https://doi.org/10.1016/j.trgeo.2021.100570.

Peck, R.B. (1969), "Deep excavations and tunnelling in soft ground", *proc.int.conf.on smfe*.

Rezaei, A.H. and Ahmadi-adli, M. (2020), "The volume loss: real estimation and its effect on surface settlements due to excavation of Tabriz Metro tunnel", *Geotech. Geol. Eng.*, **38**(3), 2663-2684.

Rowe, R. and Kack, G. (1983), "A theoretical examination of the settlements induced by tunnelling: four case histories", *Can. Geotech. J.*, **20**(2), 299-314.

Shah, R., A. Lavasan, A., Peila, D., Todaro, C., Luciani, A. and Schanz, T. (2018), "Numerical study on backfilling the tail void using a two-component grout", *J. Mater. Civ. Eng.*, **30**(3), 04018003. https://doi.org/10.1061/(ASCE)MT.1943-5533.0002175.

Sjölander, A., Hellgren, R., Malm, R. and Ansell, A. (2020), "Verification of failure mechanisms and design philosophy for a bolt-anchored and fibre-reinforced shotcrete lining", *Eng. Fail. Anal.*, **116**, 104741. https://doi.org/10.1016/j.engfailanal.2020.104741.

Swoboda, G., Kenawi, M. and Ramadan, E. (2004), "Numerical investigation of TBM tunnelling in consolidated clay", *Proc., Underground space for sustainable urban development. Proceedings of the 30th ita-aites world tunnel congress.*, Tunnelling and Underground Space Technology.

Wang, S., Liu, C., Shao, Z., Ma, G. and He, C. (2020), "Experimental study on damage evolution characteristics of segment structure of shield tunnel with cracks based on acoustic emission information", *Eng. Fail. Anal.*, **118**, 104899. https://doi.org/10.1016/j.engfailanal.2020.104899.

Xu, X.H., Xiang, Z.C., Zou, J.F. and Wang, F. (2020), "An improved approach to evaluate the compaction compensation grouting efficiency in sandy soils", *Geomech. Eng.*, **20**(4), 313-322. https://doi.org/10.12989/gae.2020.20.4.313.

Yu, Q., Zhou, H., Wang, Y. and Duan, R. (2016), "Quality monitoring of metro grouting behind segment using ground penetrating radar", *Constr. Build. Mater.*, **110**, 189-200. https://doi.org/10.1016/j.conbuildmat.2015.12.109.

Zhang, D., Xie, X., Zhou, M., Huang, Z. and Zhang, D. (2021), "An incident of water and soil gushing in a metro tunnel due to high water pressure in sandy silt", *Eng. Fail. Anal.*, **121**, 105196. https://doi.org/10.1016/j.engfailanal.2020.105196.

Zhang, F., Xie, X. and Huang, H. (2010), "Application of ground penetrating radar in grouting evaluation for shield tunnel construction", *Tunn. Undergr. Sp. Tech.*, **25**(2), 99-107. https://doi.org/10.1016/j.tust.2009.09.006.

Zhang, J., Li, S., Li, L., Zhang, Q., Xu, Z., Wu, J. and He, P. (2017), "Grouting effects evaluation of water-rich faults and its engineering application in Qingdao Jiaozhou Bay Subsea Tunnel, China", *Geomech. Eng.*, **12**(1), 35-52. https://doi.org/10.12989/gae.2017.12.1.035.

Zhao, K., Bonini, M., Debernardi, D., Janutolo, M., Barla, G. and Chen, G. (2015), "Computational modelling of the mechanised excavation of deep tunnels in weak rock", *Comput. Geotech.*, **66**, 158-171. 10.1016/j.compgeo.2015.01.020.

Zhao, T., Ding, W., Qiao, Y. and Duan, C. (2019), "A large-scale synchronous grouting test for a quasi-rectangular shield tunnel: Observation, analysis and interpretation", *Tunn. Undergr. Sp. Tech.*, **91**, 103018. https://doi.org/10.1016/j.tust.2019.103018.

GC